

pairs (P13/P14, P10.1, P8/P9) is grafted onto a similar core.

Surprisingly, the crystal structure of the ribosome as well as of other RNAs demonstrate a recurring motif: that is, long-range RNA-RNA anchors mediated by adenine bases that make contact with the shallow minor grooves of two stacked base pairs of RNA helices (14). RNA has a remarkable propensity for contributing two contiguous adenines to such A-minor interactions. Sometimes the consecutive adenines belong to GNAA tetraloops, but other RNA motifs also are able to fold with two adenines poised for binding to the shallow/minor groove of a helicoidal region. The proper conformation of these adenines is generally ensured by other local interactions involving one edge of the adenines, leaving the other edges free for further long-range interactions.

The four RNA-RNA contacts (indicated by arrows in the figure) are all mediated by A-minor interactions. Strikingly, the anchoring of the subdomains is via A-minor anchoring motifs between different peripheral domains, even though they are embedded within very different structural contexts. In type A RNA, adenines in the heptaloop L13 and the tetraloop L14 contact stacked base pairs in P12 and at the base of P8, respectively (9). But in type B RNA, adenines in the apical

loop of P12 contact a special motif in P10.1, and a single-stranded region organizes itself in a loop with two adenines contacting the stack between P7 and P10 (12). Thus, with A-minor anchoring motifs, nonhomologous peripheral elements can form different and mutually exclusive long-range contacts to promote an identical functional purpose: the stabilization of the helical stems that build the recognition core (helices P7 to P11) that correctly positions the substrate. There is increasing awareness of the structural importance of peripheral RNA domains in the evolution and function of RNAs. For example, peripheral domains of the small hammerhead ribozyme identified in sequence alignments affect its catalytic activity (13).

RNA structural bioinformatics is based on comparative analysis, which searches for coordinated events in sequence evolution to infer spatial relationships. The structural knowledge gained by comparing sequences of homologous RNAs is unequaled: All of the long-range contacts discussed above have been identified by comparative analysis (15, 16). Yet the exquisite atomic views of such contacts would not have been possible without crystallography. Furthermore, the two crystal structures offer definite clues about conserved residues (especially bulges or unpaired

regions) that were clearly seen as conserved in sequence alignments but whose role was unclear. The next challenge resides in the integration of the rich and complex three-dimensional information gained by crystallography with the ever-increasing number of sequence databases. The implication is that systematic comparisons between crystal structures and aligned sequences should tease apart the key molecular connections that maintain biologically functional RNAs. The goal is to derive the rules of molecular evolution that govern the RNA world, which forms the origin of our DNA-based modern life.

#### References

1. C. Guerrier-Takada *et al.*, *Cell* **35**, 849 (1983).
2. K. Kruger *et al.*, *Cell* **31**, 147 (1982).
3. D. P. Bartel, *Cell* **116**, 281 (2004).
4. Y. Dorsett, T. Tuschl, *Nature Rev. Drug Discov.* **3**, 318 (2004).
5. B. T. Wimberly *et al.*, *Nature* **407**, 327 (2000).
6. N. Ban *et al.*, *Science* **289**, 905 (2000).
7. P. L. Adams *et al.*, *Nature* **430**, 45 (2004).
8. F. Guo *et al.*, *Mol. Cell*, in press.
9. A. S. Krasilnikov *et al.*, *Science* **305**, 104 (2004).
10. B. D. James *et al.*, *Cell* **52**, 19 (1988).
11. A. Loria, T. Pan, *RNA* **2**, 551 (1996).
12. A. S. Krasilnikov *et al.*, *Nature* **421**, 760 (2003).
13. A. Khvorova *et al.*, *Nature Struct. Biol.* **10**, 708 (2003).
14. P. Nissen *et al.*, *Proc. Natl. Acad. Sci. U.S.A.* **98**, 4899 (2001).
15. J. L. Chen *et al.*, *EMBO J.* **17**, 1515 (1998).
16. C. Massire *et al.*, *J. Mol. Biol.* **279**, 773 (1998).

#### APPLIED PHYSICS

## Boosting Magnetoresistance in Molecular Devices

Christoph Strunk

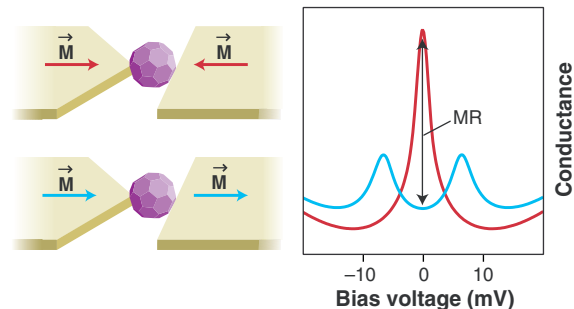
Advances in nanoelectronics continue to push forward the miniaturization of devices and the improvement of their speed and functionality. Of particular importance are the fields of molecular electronics and spintronics. By studying electronic transport at molecular scales—for example, through individual carbon nanotubes (1),  $C_{60}$  molecules (2), and single organic molecules (3)—researchers try to reach the ultimate size limits for devices. In spintronics, the spin rather than the charge is used to store and process classical as well as quantum information (4).

On page 86 of this issue, Pasupathy *et al.* (5) succeed in merging these two fields. They explore molecular quantum dots consisting of single  $C_{60}$  molecules, which

are sandwiched between two ferromagnetic nickel electrodes (see the figure). These new spintronic devices combine two fundamental electron-electron interaction effects of condensed matter physics: the Kondo effect and ferromagnetism. At first sight, these effects seem to exclude

#### Merging the Kondo effect and ferromagnetism. (Left)

Artist's view of the  $C_{60}$  quantum dot between ferromagnetic nickel electrodes. The different shapes of the electrodes enable a controlled transition between parallel and antiparallel alignment of the magnetization,  $\mathbf{M}$ . (Right) Differential conductance versus bias voltage of the device for the parallel (blue) and antiparallel state (red). For parallel alignment, the Kondo resonance is split by the exchange fields of the two electrodes. For antiparallel alignment, the exchange fields of the two electrodes cancel each other, and Kondo resonance is restored at zero-bias voltage. This leads to a large magnetoconductance MR, which exceeds the usual tunneling magnetoconductance (arrow).



each other, but they have now been integrated in one device. Once a controlled assembly of such devices is achieved, they may even outperform more conventional magnetoelectronic devices.

Previous experiments have shown that a quantum dot trapping an unpaired electron can display the Kondo effect, which is one of the most prominent many-body effects in condensed matter physics (6, 7). If the tunneling barriers defining the quantum dot are sufficiently transparent, the wave function of the single electron can leak out of the dot and hybridize with the delocalized electrons in the contacts. The Coulomb repulsion on the dot leads to an antiferromagnetic exchange

coupling between the electron spin on the dot and the neighboring electron spins in the electrodes. The corresponding coupling energy can be expressed as a characteristic temperature, the Kondo temperature  $T_K$ . Below this temperature, the spin on the dot is screened by the formation of a cloud of electrons on the electrodes, having a spin polarization antiparallel to the spin on the dot. The formation of the screening cloud enhances the density of states in the electrodes and leads to a high-conductance state. The hallmark of the Kondo effect is a pronounced peak in the differential conductance with width  $k_B T_K$  (where  $k_B$  is the Boltzmann constant), which gradually disappears at temperatures above  $T_K$ . In the presence of a magnetic field, this peak shows a Zeeman splitting.

Until recently, the prospects for using the Kondo effect in quantum dots in applications were poor because it required temperatures below 1 K. The use of molecules as quantum dots has pushed the Kondo temperature up to 30 K (8, 9). However, at this high  $T_K$ , very large external magnetic fields are required to split the Kondo resonance, again precluding applications in magnetoelectronics.

The situation is changed completely by the experiment of Pasupathy *et al.* (5). The use of

ferromagnetic electrodes puts the antiferromagnetic Kondo interaction in competition with the ferromagnetic spin alignment by the ferromagnet's exchange field. The exchange field is responsible for the spontaneous spin polarization of the ferromagnet and acts also on the single spin trapped on the quantum dot. It has an effect similar to that of an external magnetic field. However, the corresponding Zeeman energy is given by the Curie temperature,  $T_C$ , which is 20 to 30 times larger than  $T_K$ . The exchange field is much larger than laboratory-scale magnetic fields.

Moreover, in devices with symmetric coupling, the exchange fields of the two electrodes cancel each other if their magnetization is antiparallel. Hence, a huge effective magnetic field can be controlled by the tiny external magnetic fields required to switch the magnetization of the two electrodes. By virtue of the ferromagnetic hysteresis, the molecular device turns out to be a bistable switch, which can be controlled precisely in the same way as more conventional magnetoelectronic devices—with the advantage that the magnetoresistance is enhanced by the Kondo resonance and much larger than the usual tunneling magnetoresistance (see the figure).

The main drawback of the new devices is that so far, their fabrication relies on chance. Only 30 out of 1000 devices show the Kondo effect. This is typical for the current state of molecular electronics. The control of the electronic transport properties of molecular devices requires a positioning of the device components with an accuracy far better than 1 nm. The assembly of carbon nanotube field-effect transistors has been demonstrated using DNA templates (10), but does not yet allow a sufficient level of precision. Here is much scope for future developments. Nevertheless, the experiment of Pasupathy *et al.* is an important proof of principle and will fuel progress in fundamental physics, sample fabrication, and device applications.

#### References

1. S. J. Tans, A. R. M. Verschueren, C. Dekker, *Nature* **393**, 49 (1998).
2. C. Joachim, J. K. Gimzewski, R. Schittler, C. Chavy, *Phys. Rev. Lett.* **74**, 2102 (1995).
3. J. Reichert *et al.*, *Phys. Rev. Lett.* **88**, 176804 (2002).
4. S. A. Wolf *et al.*, *Science* **294**, 1488 (2001).
5. A. N. Pasupathy *et al.*, *Science* **306**, 86 (2004).
6. D. Goldhaber-Gordon *et al.*, *Nature* **391**, 156 (1998).
7. S. M. Cronenwett, T. H. Oosterkamp, L. P. Kouwenhoven, *Science* **281**, 540 (1998).
8. J. Park *et al.*, *Nature* **417**, 722 (2002).
9. W. Liang *et al.*, *Nature* **417**, 725 (2002).
10. K. Keren *et al.*, *Science* **302**, 1380 (2003).

#### GEOPHYSICS

## Are Earth's Core and Mantle on Speaking Terms?

Cin-Ty Aeolus Lee

Earth's interior is divided into a central core made of an iron-nickel alloy and a rocky mantle made of silicate and oxide minerals. Earth scientists often ignore the core in their treatments of the chemical and dynamic evolution of the mantle after core-mantle segregation. However, there has been growing debate on whether there may be significant chemical interaction between the core and the mantle. On page 91 of this issue, Humayun *et al.* (1) present data that suggest that the lower mantle may be enriched in iron compared to the upper mantle, and that this iron enrichment may indeed be due to core-mantle interaction.

If the lower mantle is enriched in iron through chemical reactions between the lower mantle and the liquid outer part of the Earth's core (2), then the dynamics of the core and mantle must be coupled. The iron enrichment will also influence the physical

properties of the lower mantle (such as its density, elasticity, and electrical conductivity). However, direct evidence for an iron-rich lower mantle is lacking. Moreover, even if the lower mantle is enriched in iron, other explanations are plausible. For example, the mantle may retain a primordial compositional stratification. Alternatively, subduction of oceanic crust or deep-sea marine sediments, some of which may be enriched in iron and manganese, may cause the enrichment.

It is widely believed that volcanic hotspots are the surface manifestations of plumes rising up from the lower mantle or core-mantle boundary. Earth scientists therefore use hotspot volcanoes as windows into Earth's deep interior. Humayun *et al.* (1) report the Fe/Mn ratios of basaltic lavas associated with a well-known hotspot, Hawaii. They show that the Hawaiian lavas have higher Fe/Mn ratios than basalts from mid-ocean ridges; the latter only tap the upper mantle (see the figure, inset).

The authors argue that the partitioning of iron and manganese between melts and

the mantle is roughly equal, and that the Fe/Mn ratio of a melt should therefore closely reflect the Fe/Mn ratio of the melt source region. They thus suggest that the high Fe/Mn ratios of the Hawaiian lavas reflect a lower mantle enriched in iron, possibly due to long-term chemical interaction between the core and the mantle.

If this interpretation is correct, then the results provide the second observational evidence for a core component to the Hawaiian mantle source. The first evidence came from anomalously high concentrations of the isotope  $^{186}\text{Os}$  in Hawaiian lavas (3), which were attributed to a Hawaiian mantle source that has incorporated small amounts of outer-core material. The latter is hypothesized to have elevated  $^{186}\text{Os}$  due to its high Pt/Os ratio and radioactive decay of  $^{190}\text{Pt}$  to  $^{186}\text{Os}$  (3). Others have argued that the  $^{186}\text{Os}$  anomalies are more likely to result from incorporation of subducted Fe-Mn-rich marine sediments (4, 5), which also have high Pt/Os ratios. However, such sediments have low Fe/Mn ratios, which is inconsistent with the high Fe/Mn ratios of Hawaiian lavas reported by Humayun *et al.* (1).

Why were the consistently high Fe/Mn ratios in Hawaiian lavas not recognized earlier, given that iron and manganese have been routinely measured for decades? Humayun *et al.* suggest that the existing database of iron and manganese in Hawaiian lavas and mid-ocean ridge basalts

The author is in the Department of Earth Science, Rice University, Houston, TX 77005, USA. E-mail: ctlee@rice.edu